Validation of Finite-Element Models using Full-Field Experimental Data: Leveling FEA Data Through a DIC Engine

P Lava*[1], EMC Jones*†[2], L Wittevrongel[1], and F Pierron[3]

[1] *MatchID NV, Ghent, Belgium*
[2] *Diagnostic Science and Engineering, Sandia National Laboratories, Albuquerque, NM, USA*
[3] *Engineering and Physical Sciences, University of Southampton, Southampton, UK*

March 23, 2020

Abstract

Full-field data from Digital Image Correlation (DIC) provides rich information for finite element analysis (FEA) validation. However, there are several inherent inconsistencies between FEA and DIC data that must be rectified before meaningful, quantitative comparisons can be made, including: strain formulations, coordinate systems, data locations, strain calculation algorithms, spatial resolutions, and data filtering. In this paper, we investigate two full-field validation approaches: (1) the *direct interpolation approach*, which addresses the first three inconsistencies by interpolating the quantity of interest from one mesh to the other; and (2) the proposed *DIC-leveling approach*, which addresses all six inconsistencies simultaneously by processing the FEA data through a stereo-DIC simulator to "level" the FEA data to the DIC data in a regularization sense. Synthetic "experimental" DIC data was generated based on a reference FEA of an exemplar test specimen. The direct interpolation approach was applied, and significant strain errors were computed, even though there was no model form error, because the filtering effect of the DIC engine was neglected. In contrast, the leveling approach provided accurate validation results, with no strain error when no model form error was present. Next, model form error was purposefully introduced via a mismatch of boundary conditions. With the direct interpolation approach, the mismatch in boundary conditions was completely obfuscated, while with the leveling approach, it was clearly observed. Finally, the "experimental" DIC data was purposefully misaligned slightly from the FEA data. Both validation techniques suffered from the misalignment, thus motivating continued efforts to develop a robust alignment process. In summary, direct interpolation is insufficient, and the proposed leveling approach is required to ensure that the FEA and the DIC data have the same spatial resolution and data filtering. Only after the FEA data has been "leveled" to the DIC data can meaningful, quantitative error maps be computed.

Keywords: Verification and Validation (V&V); Finite-Element Analysis (FEA); Digital Image Correlation (DIC); DIC-Leveling Approach

1 Introduction

Verification and validation (V&V) of finite-element analyses (FEA) is critical to building credibility and confidence in model predictions for engineering design analysis. Specifically, verification is the process of proving that the implemented model is accurately solving the governing equations for the model and that the code driving the model is correctly implemented. Validation is the process of demonstrating that the model is a valid representation of the physical system that is being simulated and can accurately predict the quantities of interest in the system. Generally verification focuses on verifying the code written to solve the

*Equal contribution authors
†Corresponding author: emjones@sandia.gov

model and investigating the numerical sensitivities of the model (e.g. discretization errors, numerical solver options, etc.); while validation focuses on determining and quantifying the influence of model physics and inputs to the model [1].

In this article, we focus on one critical step to validation for solid mechanics FEA: comparing predictions from FEA to experimental data. Historically, experimental data for validation studies was limited to either global data (e.g. resultant applied force) or point data (e.g. strain gauges and thermocouples). Such data, however, misses important details about local deformation. The resultant applied force, for instance, could agree between the model and the experiment, but the model could fail to capture strain localization accurately. This issue points towards the problem of model uniqueness, where several models or the same model with different sets of parameters could provide the same global force, which is integrative information, yet differ significantly by other metrics, such as local strain fields or evolution of internal state variables. Additionally, the location of strain gauges and thermocouples are determined based on expected deformation, but there is no guarantee that the maximum strain or temperature will occur in those locations. Alternatively, photoelasticity provides full-field validation information [2–4], but requires either a coating applied to the specimen or a 3D model constructed of a photoelastic material that is not representative of the actual material.

The maturation of techniques for measuring full-field deformation of test pieces, such as Digital Image Correlation (DIC) [5] or the grid method [6], have opened the door for richer experimental data for validation studies. In this work, we focus on DIC data, but many of the discussion points and conclusions apply also to data from the grid method. Qualitative comparisons of field data between FE simulations and experimental DIC deformation data are simple and can provide valuable information to the design engineer in the beginning stages of model development. Features such as location of strain localization and failure can be readily observed with the field data, and the approximate location of these features can be compared qualitatively to the FE predictions.

The real power of full-field experimental data, though, rests in quantitative comparisons, which allow the design engineer to assess the quality of the FE model more precisely and reduce conservative margins. One approach is to decompose the field data using a set of basis functions, and then compare the amplitudes of the basis functions between the FE model and the experimental data [7–11]. An advantage of this method is that the potentially-overwhelming amount of full-field data generated by DIC and FEA can be reduced to a more manageable format. Additionally, by using only a finite number of basis functions, the decomposition serves to filter high spatial frequency noise from the low spatial frequency signal of interest. However, determining the number of basis functions to use is somewhat arbitrary, and significant discrepancies between the DIC data and the FEA data in regions of high strain gradients could potentially be filtered along with the high-frequency noise. Another shortcoming lies in the fact that the FE model and the DIC measurements will have different spatial cut-off frequencies. Indeed, the number of finite elements can be increased at will while the number of DIC data points is limited by the fixed camera spatial resolution. Therefore, differences between FE and DIC data arising from differences in spatial convergence in areas of large gradients can be falsely attributed to model errors. Finally, at a time when engineers have now embraced data-rich design owing to the spectacular progress in computational capabilities, it is somewhat against this trend to seek to reduce the experimental data richness down to a few indicators as in [7–9].

In this work, we focus on an alternative approach in which full-field error maps of quantities-of-interest, such as strain, are computed. Before FEA and DIC data can be directly subtracted, however, there are several inconsistencies that must be addressed, including different: coordinate systems, data locations, strain formulation and calculation methods, spatial resolutions, and data filtering. A so-called direct interpolation approach, whereby the FEA and experimental data point clouds are aligned via several interpolation steps, can resolve some of these issues, but will generally fail with respect to the latter two inconsistencies, as will be shown further on.

To address all these issues simultaneously, we present a holistic method that invokes a stereo-DIC simulator [12, 13]. The simulator uses the FE mesh and FE displacements from the surface of the model to synthetically deform an image of a DIC speckle pattern. We call this process FEA-based synthetic image deformation, or F-SID, and it is an extension of a 2D-DIC simulator previously implemented by Lava et al. to investigate the influence of user-defined parameters on DIC results [14]. The synthetically deformed images can then be processed through the DIC software using the same settings as for the experimental DIC images. In this way, the FEA data is "leveled" to the DIC data, by ensuring that both sets of data have the

same filtering, spatial resolution, and strain calculation method. We call this process "DIC-leveling", and the resultant data is referred to as "DIC-leveled FEA" data. Moreover, both DIC and FEA are through this procedure subjected to the same calibration and triangulation process, directly expressing both data clouds within the same coordinate frame and yielding coincident data point locations. Hereby, additional interpolation steps can be omitted. Finally, since this approach involves a true DIC speckle pattern, many possible error sources related to the pattern itself are naturally incorporated into the leveled FEA data. As such, some image artifacts related to the pattern (e.g. aliasing, pattern defects) can be more easily disentangled from true model issues.[1]

Similar to our approach, a stereo-DIC simulator has also been included in the validation loop when comparing FEA data to global stereo-DIC data [15, 16]. One disadvantage of global-DIC, though, is that a converged FE mesh may be too small to be used for global-DIC (for example, a refined mesh around a strain concentrator). Additionally, strain computation and extraction to nodal locations depend on the element type (e.g. shell versus solid), which may not be the same for both DIC measurements and FEA. Therefore, for a meaningful comparison between experimental and FE results, the same type of leveling approach as presented here would be needed. This is beyond the scope of the current work. Since the majority of commercial DIC packages use local shape functions, it was decided to focus on local DIC here to maximize the impact of the work.

This article compares the direct interpolation approach with the DIC-leveling approach using synthetic "experimental" data generated from FEA. By using synthetic data with a known reference solution, the accuracy of the validation procedures is evaluated independently of any unknown model form error that could be present in actual experimental data. The paper is organized as follows. First, an overview of three different field comparison procedures is presented, for direct interpolation, the DIC-leveling approach, and field decomposition. Second, the method used to synthetically deform images according to FEA displacements (F-SID) is summarized. Third, the exemplar case is presented, including the methods used to generate the FEA and the synthetic "experimental" DIC data. Finally, full-field validation results are discussed in depth for both the direct interpolation and the DIC-leveling approach, and effects of processing parameters, model form error, and mesh alignment are all investigated. Overall, the methods described here facilitate quantitative comparisons of field data, namely strain, between FE predictions and validation DIC measurements. Details of these methods are critical for accurate validation results.

2 Field Comparison Procedures

Given two sets of full-field data, one from an FE analysis and one from an experiment (e.g. digial image correlation data), the goal of these field comparison procedures is to produce quantitative, full-field error maps for validation of the FE model. In this section, we present a synopsis of three different methods for computing the error maps. The quantity of interest could be any field data, such as displacements, velocities, accelerations, strains, strain rates, etc., but we focus on strain for demonstration purposes.

2.1 Method 1: Direct Interpolation + Direct Subtraction

Generally, quantitative comparisons between two 3D point clouds (e.g. FEA and experimental DIC results on the surface of a specimen) require three important pre-processing steps to rectify major inconsistencies between the two sets of data:

Strain formulations: Ensuring that the FEA data and the experimental DIC data have the same formulation is trivial, as both analyses have the ability to compute the strain according to a desired formulation (e.g. Green-Lagrange, Hencky). However, the default strain formulation is typically not the same for each software. Therefore, it is critical that the FE analyst and the experimentalist communicate and compare the same strain metric.

Coordinate systems: The default coordinate system for stereo-DIC data is typically related to the stereo-system calibration parameters, and inherently is completely unrelated to the coordinate system used

[1] Other artifacts that may be present in the experimental images (e.g. saturated pixels coming from specular reflections) are not currently taken into account explicitly, but are folded into the strain noise floor.

in the FEA. A coordinate transformation is required to align the experimental DIC coordinate system to that of the FEA or vice versa. This can be accomplished by registering one set of data to the second set of data using common fiducials in each data set.

Data locations: The locations of data points in the DIC data is completely unrelated to the FEA mesh. Data can be transferred from the DIC nodes to the FEA mesh or vice versa through interpolation. For instance, the shape functions employed in a FEA can be used to interpolate nodal or elemental data from the nodes or Gauss points to any arbitrary point within the element. Alternatively, a polynomial could be fit around a local region and evaluated at any arbitrary point within the region. Both methods, however, might introduce additional approximation error sources in bringing one map to the other.

Once the two sets of data use the same strain formulation, are in the same coordinate system and are evaluated on the same mesh or at the same spatial locations, the quantities-of-interest can be directly subtracted at each point in the data sets, producing full-field error maps. However, the primary aim of this paper is to illustrate that this type of direct interpolation fails to rectify other important inconsistencies between DIC and FEA data, namely different strain calculation methods, spatial resolutions, and data filtering. This is highlighted in Sec. 2.2.

2.2 Method 2: DIC-Leveling Approach + Direct Subtraction

In addition to the strain formulation, coordinate system and mesh, there are several other key inconsistencies between FEA and DIC data that we argue should also be rectified before computing full-field error maps:

Strain calculation algorithms: FEA uses shape functions of elements while DIC typically uses a polynomial fit to a local region of data. These different strain calculation algorithms can lead to different strain values, even if the underlying strain field is nominally the same.

Spatial resolutions: The spatial resolution of FEA depends on the mesh size, order of the shape function, etc., and is adjustable at will, limited only by computing power. In contrast, the spatial resolution for DIC depends on the pattern feature size, camera and lens resolution, step size, subset size, strain window, etc., and is often physically limited by camera and lens hardware and the ability to create an appropriately sized pattern.

Data filtering: DIC processing is a type of low-pass filter that may underestimate sharp displacement and/or strain gradients and that filters high spatial-frequency noise. Ignoring this filtering effect can lead to incorrect strain errors when comparing DIC data to FEA, as will be shown in this article.

We propose a second approach to quantitative comparisons of full-field data (e.g. strain), which addresses the issues of different strain calculation methods, spatial resolutions, and data filtering that are embedded in the direct interpolation approach. The key to this DIC-leveling approach is to process the FE data through the same DIC machinery as the experimental data, so that the FEA data is "leveled" to the DIC data from a regularization perspective. This is achieved by using the FEA-based synthetic image deformation (F-SID) procedure that is described in Sec. 3 to produce synthetically-deformed DIC images based on the nodal displacements from the FE model. These synthetically-deformed images are then processed using the same DIC software and DIC user-defined parameters as were used for the experimental data. The leveling approach is outlined in the flow chart in Fig. 1. The complete process is fully implemented in the FE Deformation Module (to synthetically deform the images) and the FE Validation Module (to processes the synthetically deformed images and compute strain error maps) in MatchID.

This leveling process serves to apply the same filtering to both the FE displacements and the DIC displacements (through the DIC-simulator), to ensure that the same definition of strain was used for both sets of data, and to address the issue of differing spatial resolution since the spatial derivatives were computed over the same length scale in each set of data. Moreover, identical regions of interest and initial subset locations are imposed on both the experimental and synthetic reference image, hereby naturally answering the data locations question avoiding additional interpolation steps. With the differences in data processing between the two sets of data rectified, the quantitative validation has improved accuracy compared to the direct interpolation method, as discussed in Sec. 5.

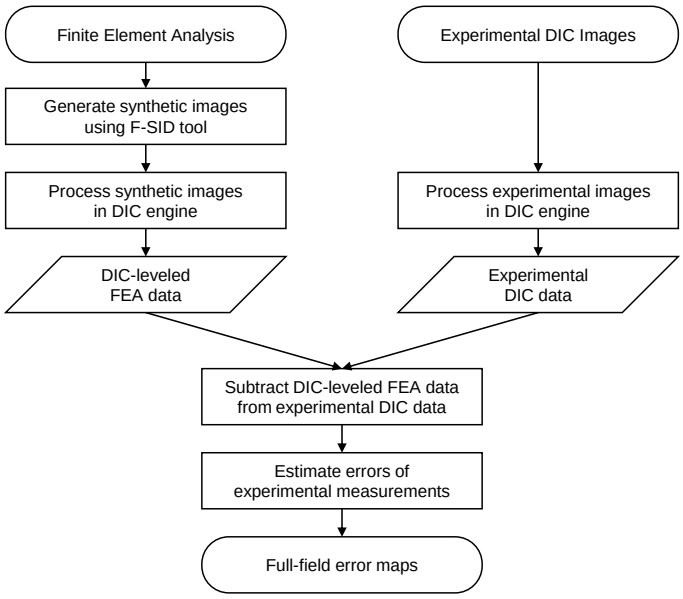

Figure 1: Flow chart demonstrating the main steps in the DIC-leveling approach to compute full-field error validation maps.

One could argue that the generation of full-field error maps through the synthetic image deformation procedure might be computationally expensive. The implemented algorithms in MatchID, however, are highly parallelized and optimized. As a reference, with a 2.2 Ghz QuadCore with 8 GB DDR2, the following computation times have been observed: for a 5 MPx image (2592 $\times$ 1944 px) with a mesh density of 4 $\times$ 4 pixels (and accordingly approximately 30k elements), one pair of stereo images takes approximately 2.7 secs. The numerical deformation does not exponentially scale with the image dimensions, nor with the mesh density. Accordingly, this is very minor in view of the large computational times sometimes involved in running the FE simulation itself.

2.3 Method 3: Field Decomposition

A third approach to comparing field data is to decompose the data into different mode shapes with associated amplitudes by projecting the data onto a set of basis functions [7–11]. While this approach is not explored in depth in the current article, we present a brief discussion on it. Like the direct interpolation method (Sec. 2.1), the quantity of interest (e.g. strain) is computed independently in the FEA and in the experimental DIC data, and each set of field data is fitted to the basis functions separately. Thus, the decomposition technique, in its most straight-forward application, suffers from the same discrepancies regarding different strain calculation algorithms and spatial resolutions. Examples of false positives and false negatives generated from this approach were exhibited in [17]. Earlier works [7–9] used Zernike, Tchebichef, or Krawtchouk polynomials, restricting the region-of-interest to be rectangular or circular, a strong limitation of the technique. More recently, Alpert wavelets have been applied for the decomposition [10, 11], which allows the method to be generalized to any arbitrary geometry. As with the DIC-leveling approach (Sec. 2.2), the synthetic image deformation technique (Sec. 3) could be used to level the FEA field data to the experimental DIC data first. Then, the two sets of field data, which now have the same spatial resolution, can be decomposed onto the basis functions. By including the DIC-simulator in the loop, a more fair comparison is obtained. A thorough investigation of the effect of the DIC-simulator on the field decomposition process is reserved for a future study.

3 FEA-Based Synthetic Image Deformation (F-SID)

An integral concept to the DIC-leveling approach for comparison of field data is the generation of synthetically deformed speckle images for DIC, based on FEA nodal information, which we call F-SID. The image deformation procedure is detailed in [18], while the extension to stereo-DIC is reported in [12]. The stereo-DIC simulator has been implemented in the FE Deformation module of the commercial software MatchID. F-SID is a subset of other synthetic image deformation techniques based on, for example, analytical expressions [19, 20].

Here, we briefly repeat the basic underlying principles, which are shown in Fig. 2. First, a finite-element simulation is performed yielding a mesh with corresponding nodal locations in the reference (unloaded) configuration. This mesh is then aligned with and imposed onto an image of a DIC pattern captured by the left stereo DIC camera (annotated camera 0). Various deformed configurations generated by the FEA solver generate then nodal displacements that can be invoked to retrieve grey values at non-integer pixel locations: $(x+u, y+v)$, with (u, v) determined from the shape functions of the element the pixel belongs to. Next, a set of intrinsic and extrinsic camera parameters — as derived in a true experiment — project the FEA nodal locations from the camera 0 sensor plane to the sensor plane of camera 1, yielding grey values at non-integer pixel locations $(x+u+q, y+v+r)$, with (q, r) the additional projection displacements. For both camera 0 and camera 1, eventual lens distortions can be taken into account, additionally displacing the grey level locations according to the underlying distortion model.

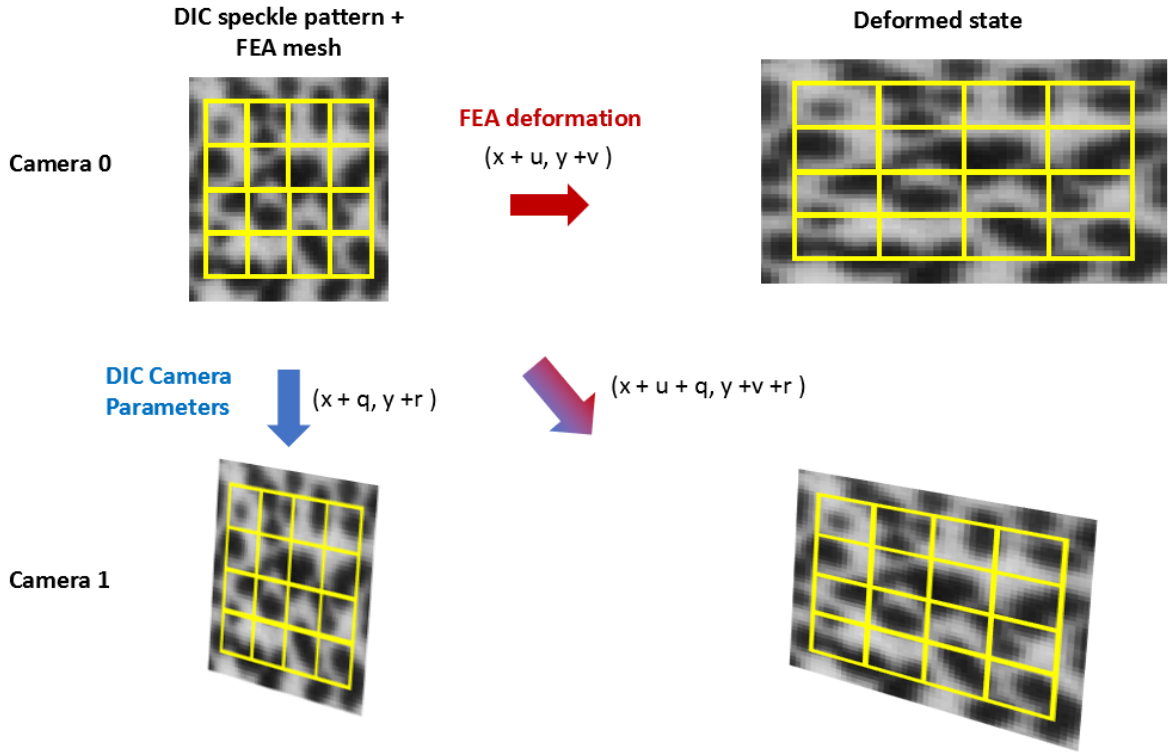

Figure 2: Illustration of the procedure used to synthetically deform images of a DIC pattern according to FEA displacement data.

The actual numerical images with grey values at integer pixel locations are then constructed based on these non-integer pixel location maps. To that purpose, finite element mapping functions based on Lagrange polynomials are adopted. As such, this image deformation methodology only involves one interpolation step [12]. Moreover, since this is a reverse mapping scheme, the Lagrangian nature of DIC is naturally guaranteed [21]. Additionally, the deformation process can be adopted with a high-resolution image followed by a subsampling procedure, as illustrated in [18]. Accordingly, possible bias errors related to this image

deformation process are reduced to a maximal extent. In the end, the error introduced to the underlying FEA data through the synthetic image deformation process is typically less than 0.005 pixel [18], which is well below the typical noise floor of ca. 0.01 pixel of a well-controlled DIC measurement in the laboratory. Given these considerations, the synthetically-deformed images encode nearly exactly the underlying FEA. These images may serve a variety of purposes, such as exploring the effects of user-defined parameters in the DIC software [14], optimizing the choice of DIC parameters for material identification [18, 22–24], or designing new test configurations [25]. Here, we focus on using F-SID as one step of the DIC-leveling process for FEA validation studies.

4 Studied Case

The test specimen investigated to demonstrate the different field comparison procedures was a cover plate of a pressure vessel, shown in Fig. 3. The cover plate had a diameter of 100 mm, thickness of 1 mm, with a central tube connector of 10 mm diameter. It was clamped via bolt connections along the plate circumference and pressurized on the back side to 10 MPa. Both the bolts and the central tube connection resulted in local strain concentrations.

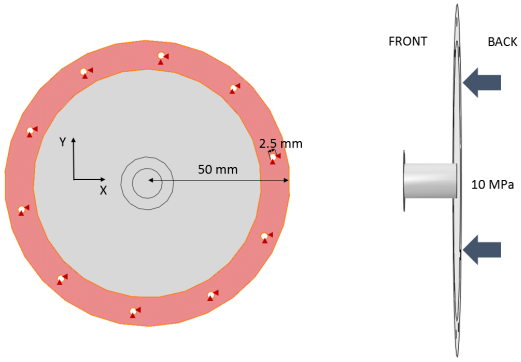

Figure 3: Geometry and loading of the pressure vessel cover.

Three sets of data were generated for this test specimen: (1) computational simulation data directly from FEA, which is used for the direct interpolation approach, (2) DIC-leveled FEA data, which is the original FEA data leveled to the experimental DIC data through a DIC simulator, used for the leveling approach and (3) synthetic "experimental" DIC data, based on the FEA, but treated as though it came from an actual experiment in the laboratory. By creating synthetic "experimental" data, with a known reference solution from the underlying FEA, different aspects of the validation process can be objectively evaluated, independent of unknown model form error that may occur with actual experimental data. Fig. 4 presents an overview of the steps used to generate the three sets of data, and details on the methods are described below.

The commercial software Abaqus was used to simulate the deformations of this component in 3D. S4R elements were adopted with hourglass control. The elements had approximate dimensions of 0.2 $\times$ 0.2 mm, resulting in converged displacements at the nodal locations and strain fields at the Gauss points. The benchmark model parameters assumed for isotropic linear hardening are presented in Table 1. This FEA is the input for all three sets of data, as shown at the top of the flowchart in Fig. 4.

In step 1, the nodal locations (X,Y,Z) and the nodal displacements (U,V,W) from the FEA were exported from Abaqus. Note that in typical validation studies using the direct interpolation approach to compare full-field strain data, the strains computed in FEA at the Gauss points of the elements would also be exported from the FEA software. However, instead of using the strains computed in Abaqus, we recomputed the strains from the displacements, as described in step 7.

In step 2, the FEA mesh was imposed onto an image of a DIC pattern corresponding to Camera 0, or the left camera, as shown in Fig. 5. This reference speckle pattern was numerically created with image resolution of 1624 $\times$ 1234 pixels. The reference speckle pattern had a minimum speckle sampling of 3 pixels, to ensure

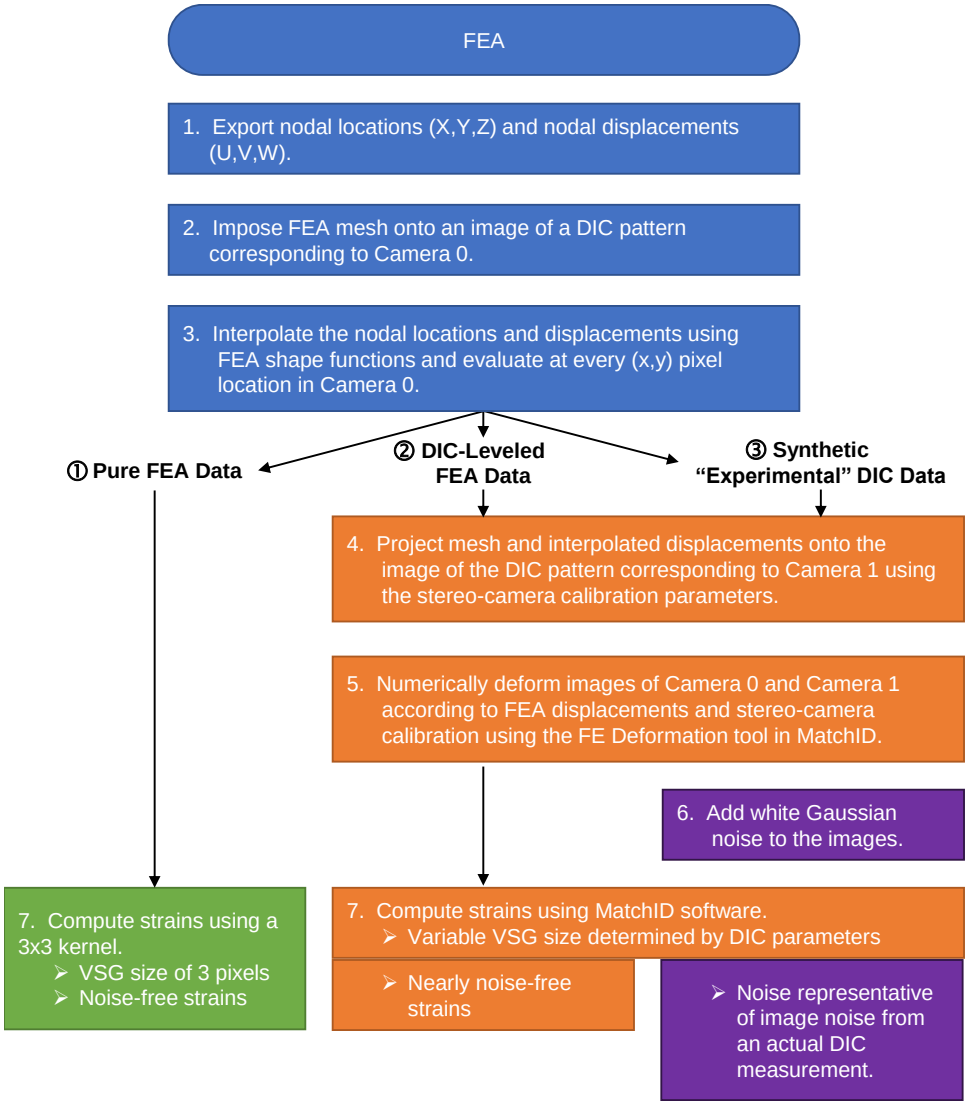

Figure 4: Overview of the steps used to generate FEA strain data, DIC-leveled FEA strain data, and synthetic "experimental" DIC strain data.

Table 1: Benchmark FE model parameters for the studied case.

Parameter	Value
Young's modulus	210 GPa
Poisson's ratio	0.3
Yield stress	500 MPa
Hardening modulus	3 GPa
Loading pressure	10 MPa

that the speckles were not aliased [26]. In typical validation studies, the FEA mesh would be aligned on the actual experimental DIC images of the test specimen, opposed to a numerically-generated image. This registration step would be accomplished through the use of fiducials present in both sets of data, or based on aligning the sample geometry represented in each set of data, and correct alignment of the FEA mesh with the experimental DIC images would be crucial at this point in the process. However, for the present study, we guarantee perfect alignment as described later. Therefore, at this point, the FEA mesh is simply centered on the DIC image.

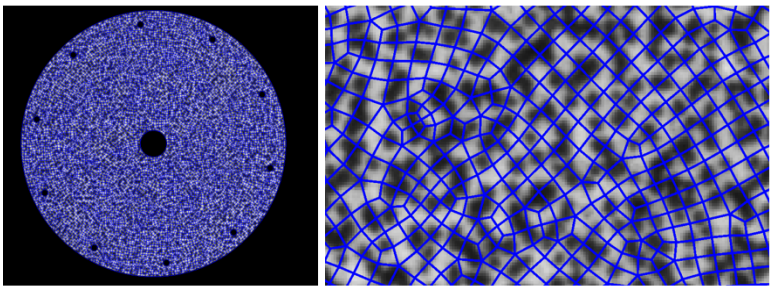

Figure 5: FEA mesh imposed onto a DIC pattern image.

In step 3, the FEA shape functions are used to interpolate the nodal locations (X,Y,Z) and the nodal displacements (U,V,W) onto every pixel location (x,y) of the Camera 0 image. Similar to step 1, for typical validation studies using the direct interpolation approach, the strains, rather than the displacements, would be interpolated onto the pixel locations. However, in the current study using synthetic data, we only need to interpolate the displacements as we will recompute the FEA strains. These first three steps are common to the FEA data, the DIC-leveled FEA data, and the synthetic "experimental" DIC data.

In step 4, for the DIC-leveled FEA data and the synthetic "experimental" DIC data, the FEA mesh and interpolated displacements were projected from the Camera 0 image to the Camera 1 image using stereo-camera calibration parameters from a representative, standard stereo-DIC setup with a 50 mm focal-length lens. These parameters are summarized in Table 2, where c_x and c_y are the calibrated coordinates of the center of the camera detector, f_x and f_y are the calibrated focal length of the lens along two directions, f_s is the skewing factor of the sensor array, κ_1 is the first-order lens distortion parameter, θ, ϕ, and ψ represent the angle of the two cameras with respect to each other about three axes, and T_x, T_y, and T_z represent the distance between the two cameras in three directions.

Table 2: Calibration parameters for the stereo-vision system for the studied.

Intrinsic	Camera 0	Camera 1	Extrinsic	
c_x (pixels)	812	812	θ (°)	0
c_y (pixels)	617	617	ϕ (°)	20
f_x (pixels)	12000	12000	ψ (°)	0
f_y (pixels)	12000	12000	T_x (mm)	-552.71
f_s (pixels)	0	0	T_y (mm)	0
κ_1	-0.4	-0.5	T_z (mm)	-53.33

In step 5, the reference speckle image, calibration parameters, and the nodal displacements from the FEA were all input into the FE Deformation module in the commercial software MatchID, which implements the synthetic image deformation procedure. The module synthetically deformed the reference image according to the FEA data, yielding images for both stereo cameras and for each load step in the FEA.

In step 6, for the synthetic "experimental" DIC data, grey level noise was added to the images to make the simulation more realistic. A simplified camera noise model, namely white (homoscedastic) Gaussian noise with a standard deviation of 0.5% of the camera dynamic range, was used, which is typical for a high-quality CCD sensor. The heteroscedastic noise profile of the camera to be used for DIC measurements could be evaluated experimentally, but this level of fidelity was not necessary for the present work. Note that this camera noise was only added to the synthetic "experimental" DIC images; for the DIC-leveled FEA data, no noise was added.

Table 3: Stereo-DIC settings used for the synthetic "experimental" DIC data and the DIC-leveled FEA data.

Field-of-View	100 mm^2
Image Scale	8 px/mm
DIC Software	MatchID
Image Pre-Filtering	Gaussian, 5 px kernel
Subset Size	21 pixels
Step Size	3 pixels
Correlation Criterion	Zero-normalized sum of square differences (ZNSSD)
Interpolant	Bicubic spline
Subset Shape Function	Affine
Strain Shape Function	Polynomial bilinear
Strain Convention	Log. Euler-Almansi

Finally, in step 7, the strains were computed for all three sets of data. For the DIC-leveled FEA data and the synthetic "experimental" DIC data, the DIC images were processed and strains were computed in MatchID with the settings shown in Table 3. For the pure FEA data, there are two possible methods for computing strains. In the first method, the strains computed natively in Abaqus are reported at the Gauss points of the elements. To compare the pure FEA data to the DIC-leveled FEA data and "experimental" data, it is imperative that strains are reported at coincident (X, Y, Z) locations for all three sets of data. Therefore, the pure FEA strains must be transferred from the Gauss points to pixel locations where the DIC-leveled FEA data and "experimental" DIC data are reported, using a polynomial or spline interpolation kernel. A second approach to calculating the pure FEA strains, which also guarantees that the strains are reported at the same (X, Y, Z) locations for all three sets of data, is to use a two-dimensional central difference interpolation of the pure FEA displacements that were previously interpolated to pixel locations in step 3. Both methodologies yield a marginal amount of smoothing, of comparable magnitude, on the final strain results. In this work, we adopted the latter technique, which results in the FEA strains being calculated over a 3×3 pixel^2 area, and reported at pixel locations in the image. Even though these strains were computed outside of Abaqus, they are used as a direct proxy for the pure FEA strains.

At the end of this process, three sets of full-field strain data were generated: (1) pure FEA strains, which were noise-free, and had a virtual strain gauge (VSG) size of 3 pixels; (2) DIC-leveled FEA strains, which were also nearly noise free,[2] but which had a VSG size determined by the DIC processing parameters; and (3) synthetic "experimental" DIC strains, with typical camera noise included, and which also had a VSG size determined by the DIC processing parameters. Here, we define the VSG size to be equal to the area of the image that is used to calculate the strain at a single location. For the synthetic "experimental" strains and the DIC-leveled FEA strains, the VSG size is given by Eqn. 1, where L_{VSG} is the size of the VSG in pixels, L_{step} is the step size in pixels, L_{subset} is the subset size in pixels, and L_{window} is the strain window in data points [26, 27].

[2]The DIC-leveled FEA strains do contain some noise due to interpolation in the F-SID process and imperfections in the matching process in the DIC engine [18]. However, camera noise is a dominant source of noise in experimental DIC measurements, and thus the DIC-leveled FEA strains are considered nearly noise-free compared to the "experimental" DIC strains.

$$L_{VSG} = (L_{window} - 1)L_{step} + L_{subset} \tag{1}$$

All sets of strain data were evaluated at pixel locations in the reference Camera 0 image: the pure FEA strains were evaluated at every pixel, and the DIC-leveled FEA strains and the "experimental" DIC strains were evaluated at a downsampled number of pixels based on the step size. Additionally, the exact same mesh alignment was used for all sets of strains in step 2. These two considerations result in a natural and inherent alignment of the three sets of data. This exact alignment is critical for the current study, to ensure that misalignment issues do not obfuscate the comparison of the direct interpolation approach and the DIC-leveling approach. We stress that the process described here to ensure alignment is typically not applicable to real experimental data. Effects on the validation results caused by misalignment are discussed in Sec. 5.4.

For the direct interpolation comparison method (Sec. 2.1), the strain error maps were computed directly by subtracting the pure FEA strains from the "experimental" DIC strains. For the DIC-leveling approach (Sec. 2.2), the strain error maps were computed by subtracting the DIC-leveled FEA strains from the "experimental" DIC strains.

5 Results and Discussion

Using the FEA data and the synthetic "experimental" data, we performed validation studies using either the direct interpolation method (Sec. 2.1) or the DIC-leveling approach (Sec. 2.2). Here, we present the results and discuss the merits and drawbacks of each approach. For demonstration purposes, the comparison is performed on the first principal strain as the quantity of interest, since strain captures details of the material behavior for this particular example. However, the comparison process is general for any field quantity-of-interest, such as displacements, velocities, accelerations, strains or strain rates.

5.1 Strain Resolution and Noise Floor

Both the DIC-leveled FEA images and the synthetic "experimental" DIC images were processed using three different virtual strain gauge (VSG) sizes. As mentioned previously, the DIC-leveled FEA data is considered to be noise free, since no camera noise was added to the synthetic images. The strain resolution of the "experimental" DIC data was evaluated from the correlation of two static images, each containing its own independent copy of white noise, and is presented in Table 4. As expected, the resolution decreases (improves) with increasing VSG size, as the larger VSGs filter out more of the random noise.

In all the results presented in the following sections, both the absolute strain error as well as the strain error normalized by the "experimental" strain resolution (Table 4) are shown. The normalized strain error maps were thresholded, so that all errors greater than 4.2 times the "experimental" strain resolution are colored red to indicate a meaningful error and thus negative validation; all errors smaller than 4.2 times the "experimental" strain resolution are colored as a multiple of the strain resolution and represent non-significant error and positive validation. The threshold value of 4.2 is selected in view of the number of data points ($\approx 40k$), hereby guaranteeing a 99.9% confidence margin.

Table 4: Strain resolution for different virtual strain gauge (VSG) sizes for the synthetic "experimental" DIC data.

VSG Size	Strain Resolution
27 px (3.3 mm)	376 µm/m
51 px (6.4 mm)	107 µm/m
93 px (11.6 mm)	32 µm/m

5.2 Direct Interpolation versus the DIC Leveling Approach

Fig. 6 presents the pure FEA major principal strain and the "experimental" DIC major principle strain computed using the three different VSG sizes. Additionally, the strain error maps were computed via direct

interpolation plus direct subtraction (Sec. 2.1). Recall that the synthetic "experimental" data encoded the exact FEA displacements. Therefore, one expects that this trivial validation study would show a positive validation (i.e. zero strain error), since there is no model error. Instead, we observe misleading negative validation results, which suggest that the "experimental" data does not agree with the FEA. Specifically, large strain errors occur near all the bolt holes where the strain gradients are large. These false errors are caused by the "experimental" DIC strains having lower spatial resolution than the FEA strains, leading to an underestimation of the peak strain in the "experimental" DIC data compared to the true strain values in the FEA data.

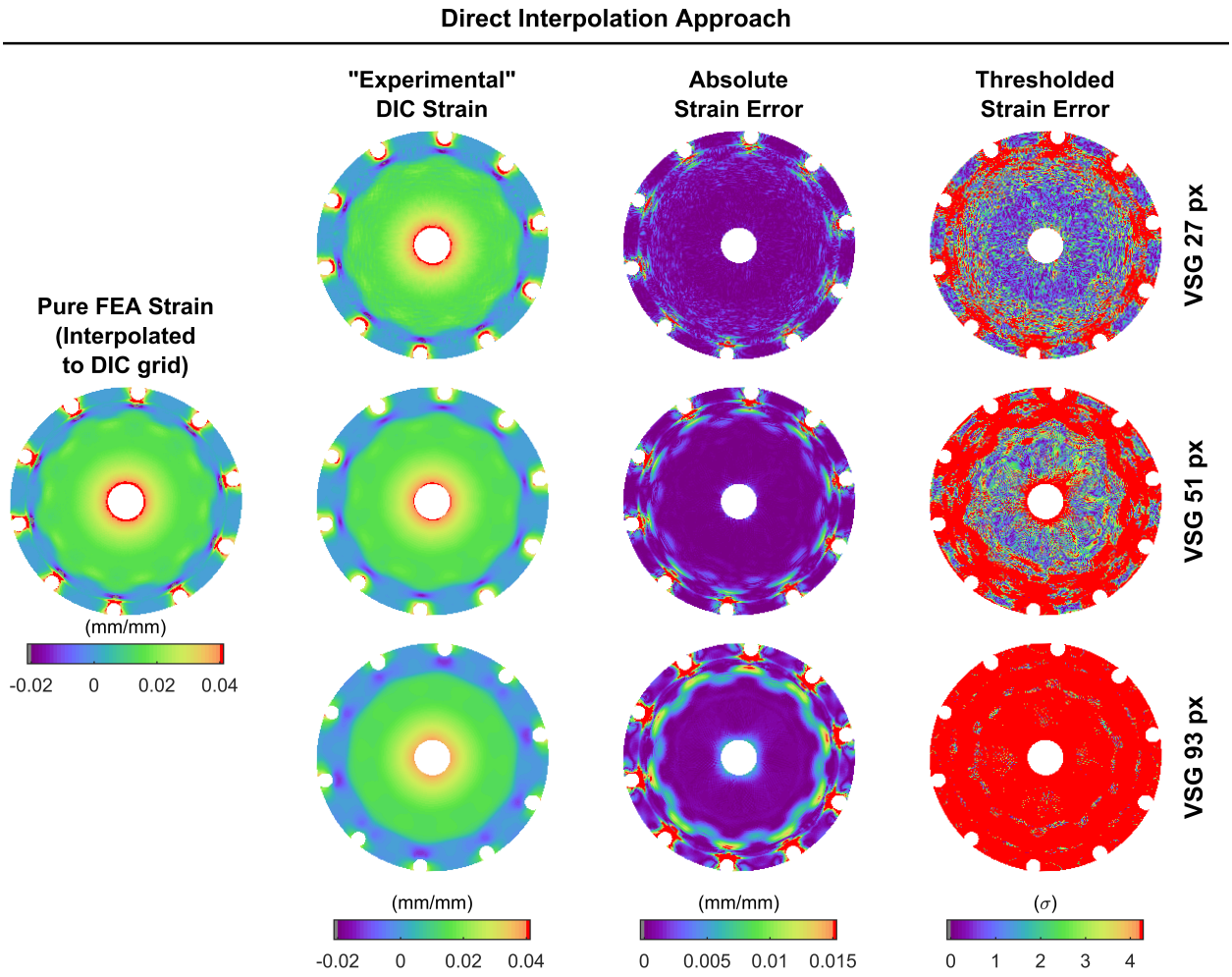

Figure 6: False negative validation results when the synthetic "experimental" DIC data is compared to the pure FEA results using direct interpolation, without taking into account the different spatial resolutions of the two sets of data and the low-pass filter effect of the DIC machinery.

Moreover, the validation results are dependent on the VSG size used in the DIC processing. Interestingly, the DIC parameters that provided the most correct validation (VSG size of 27 px), also resulted in the largest levels of random error or the highest resolution (Table 4). The temptation is often to produce smooth results, so that the experimental data "looks like" the FE data. However, in the case presented here, the systematic error dramatically increases when the "experimental" data is over-smoothed. The presence of this systematic error is often ignored, as it cannot be easily approached without modeling. It is a case of type 2 error as per the GUM [28].

Fig. 7 presents the DIC-leveled FEA strain (from the FE data processed through the DIC engine) and

the "experimental" DIC strain. Additionally, the strain error maps are shown, where the strain error was computed using the leveling approach plus direct subtraction described in Sec. 2.2. From the contours of the strain fields, we observe that both the DIC-leveled FEA strain and the "experimental" strain fields have the same filtering applied as the VSG size increases. Despite this change in filtering, the validation maps all show predominant agreement between the "experimental" data and the DIC-leveled FEA data.[3] Thus, the FE model is correctly validated. This result is in direct opposition to the false negative validation result shown in Fig. 6, when the direct interpolation strain comparison method was used.

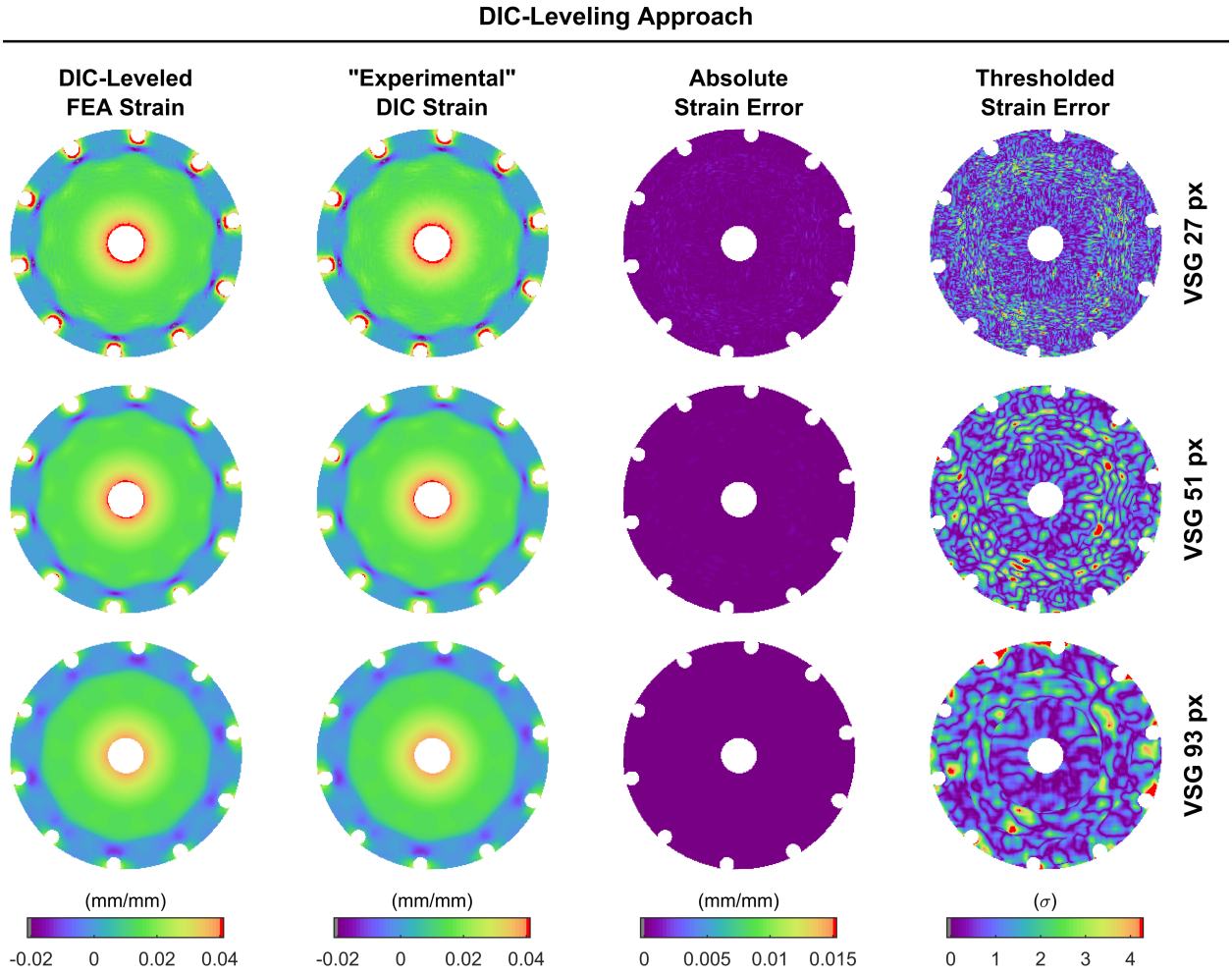

Figure 7: Accurate validation results, that are insensitive to the VSG and other DIC machinery filtering, when the FEA data is processed through the DIC machinery, and the synthetic "experimental" DIC data is compared to the DIC-leveled FEA data.

[3]The small areas of the sample that contain errors higher than 4.2 times the strain resolution (colored red in the thresholded strain error contours in Fig. 7) indicate that a more realistic estimation of the noise threshold needs to be established. That is, the strain resolution computed from two static images represents a lower bound of the actual noise floor, since it probes only effects of random camera noise and neglects effects of bias errors. In the current work with synthetic "experimental" images, the main bias error that is neglected is interpolation bias from the subset interpolant. In actual experimental images, other biases may exist, such as uncorrected lens distortions, heat waves, and equipment vibrations, to name a few. To evaluate the strain resolution more profoundly and accurately, one can rigidly translate and rotate the specimen within the field-of-view and depth-of-field of the two cameras, and compute the mean and standard deviation of the strains calculated from these rigid-body-motions. A full determination of the exact noise floor, however, is a cumbersome and intense uncertainty quantification process that is beyond the scope of this work and is subject to further research (see for example [29]).

These results highlight the fundamental issue with directly comparing FEA strains and DIC strains. Namely, the DIC engine acts as a low-pass filter, reducing strains in localized regions of high strain gradients. If this filtering is not accounted for in the FEA strain data, an apparent model error is found during the validation studies, even when no model error is present. This result could lead an analyst to incorrectly conclude there is an issue with the FEA. However, when the leveling approach is used, the same filtering is applied to both the experimental and the FEA data, and no false errors are computed. This allows an analyst to draw correct conclusions regarding the validity of the FEA.

5.3 Effect of Model Form Error

In general, the main goal of performing a validation study is to elucidate if there is any model form error in the FEA. There are several sources of potential model form error, including inaccurate material model form, inaccurate material model parameter values, incorrect boundary conditions, low-fidelity model geometry, and non-converged FE mesh size, to name a few. Here, we examine the effects of model form error on the full-field strain maps by introducing a boundary condition mismatch between the FEA and the "experimental" data. This represents an all-too-common situation, in which idealized boundary conditions are applied to a finite-element model, but in reality, experimental boundary conditions in the laboratory are not ideal. Even a small mismatch in boundary conditions can dominate the full-field error maps generated during a validation study. To demonstrate this concept, we recreated the synthetic "experimental" DIC data, this time allowing one of the bolts to move 0.1 mm instead of constraining it fully in the base FEA. This process mimics experimental conditions when one bolt is not fully torqued. We then compare these "experimental" results with the loose bolt to the FE results with ideal boundary conditions (i.e. with all bolts fully constrained).

Fig. 8 shows the absolute and thresholded strain error maps, computed with either the direct interpolation approach or the DIC-leveling approach. Three different VSG sizes were used for the "experimental" and DIC-leveled FEA data. When the direct interpolation approach is used, the strain error maps are nearly axisymmetric, in both the absolute and thresholded maps. There is no obvious effect of one bolt having incorrect boundary conditions in the "experimental" data. Instead, the error maps are dominated simply by neglecting the filtering effect of the DIC machinery, and the error maps are nearly identical to those presented in Fig. 6, which had correct boundary conditions. Thus, if the direct interpolation approach is used, the error maps would not be useful in helping the analyst to determine the cause of the discrepancy between the model and the experiment.

In contrast, when the DIC-leveling approach is used, the absolute strain error near the loose bolt (marked by the arrow) is higher than the error in the rest of the specimen, and this holds for all three VSG sizes. Similarly, the thresholded strain error also shows the most error near the loose bolt. These results clearly indicate that there is a localized discrepancy between the model and the "experiment". This type of information is useful for the analyst to understand the cause of the discrepancy in an effort to improve the FE model.

One interesting note is that the thresholded error maps from the DIC-leveling approach here are no longer independent of the VSG size as they were in Fig. 7, which had correct boundary conditions. Instead, the larger the VSG, the more contaminating the effect of the loose bolt; the smaller the VSG, the more isolated the effect. Indeed, a small VSG will treat possible error sources more locally, whereas a larger VSG will result in a more global effect. Additionally, this dependency is related to the fact that we are thresholding the error maps based on the "experimental" strain resolution or noise floor (see Table 4). In the case of the synthetic "experimental" data used here, the noise floor is driven primarily by image noise; in actual DIC measurements in the laboratory, the noise floor could additionally include effects of vibrations, lighting fluctuations, heterogeneous index of refraction changes, to name a few. If there is a large bias error caused by something not accounted for in the noise floor, then thresholding by the noise floor will not give identical results for all VSGs. While we have demonstrated this result in the case of a bias error caused by incorrect boundary conditions, we believe a similar result would be obtained with any model form error, such as assuming an isotropic model when the material is actually anisotropic, or neglecting rate- or temperature-effects when the material is actually rate- or temperature-dependent. Despite the dependence of the thresholded error map on the VSG, the error maps still clearly indicate a localized error around the loose bolt, in contrast to the error maps obtained with the direct interpolation method.

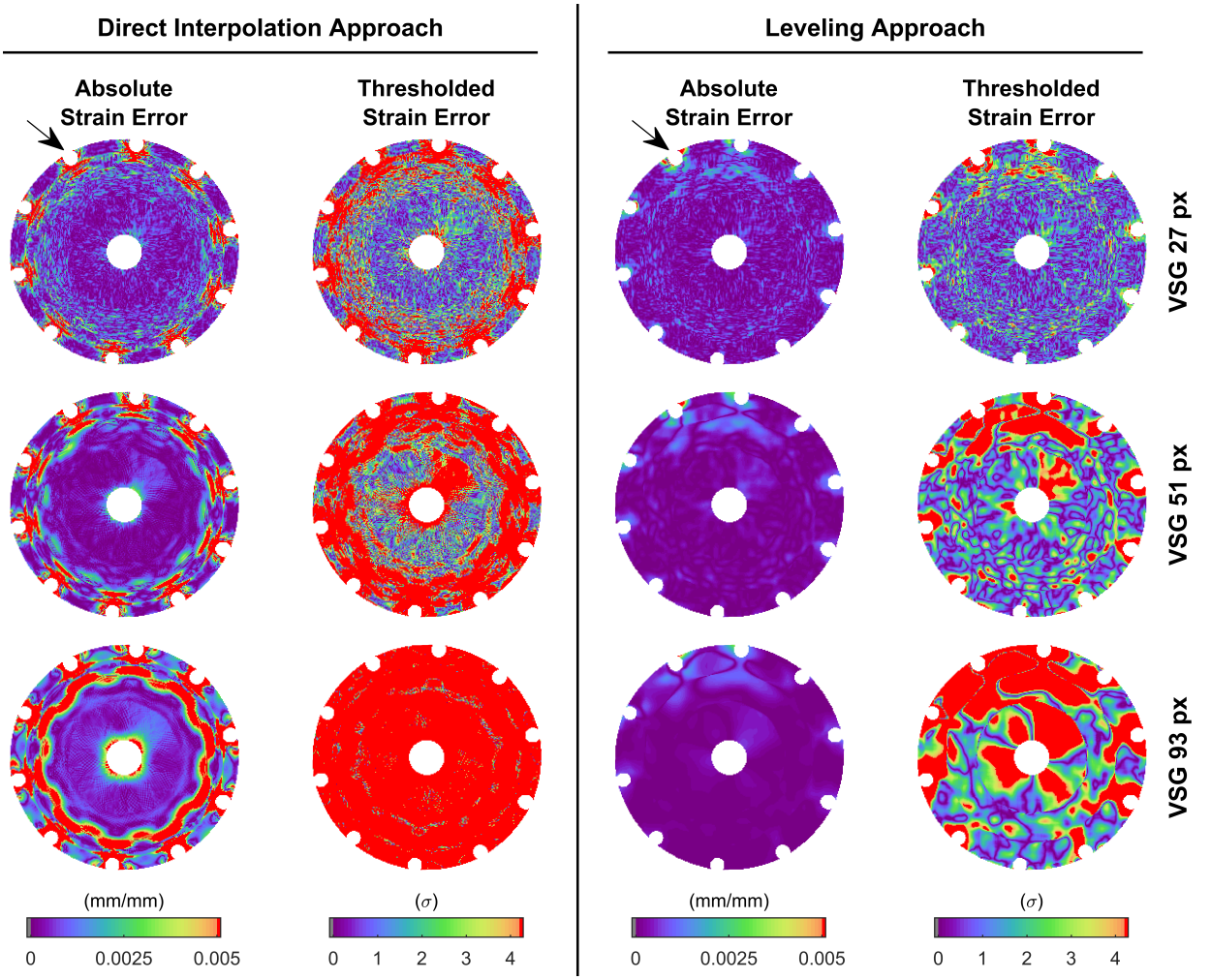

Figure 8: Effect of incorrect experimental boundary conditions on full-field strain error maps, computed with either the direct interpolation approach or the leveling approach, for three different VSG sizes. The arrows mark the bolt in the top-left that was not fully constrained.

5.4 Effect of Misalignment

In the generation of the synthetic data used in the current study, great care was taken to ensure that the pure FEA data, the DIC-leveled FEA data, and the synthetic "experimental" DIC data were all perfectly aligned, as described in Sec. 4. With actual experimental data, however, such exact alignment cannot be guaranteed. Therefore, we explore here the effect of misalignment on the strain error maps. For demonstration purposes, the pure FEA and the DIC-leveled FEA data were translated by 3 px to the right and 3 px down with respect to the "experimental" data, for a total misalignment of 4.2 px radially at a 45^o angle. Given an image scale of approximately 8 px/mm (Table 3), this misalignment corresponds to 0.52 mm, less than 1% of the diameter of the pressure vessel cover. This level of precision is reasonable for actual experimental data.

Fig. 9 presents the absolute and thresholded strain error maps for both the direct interpolation approach and the DIC-leveling approach when FEA and "experimental" data are misaligned. A VSG of 27 px was used for both the "experimental" and the DIC-leveled FEA data. Even such a small misalignment has surprisingly large effects on the strain error maps. Most noticeably, there is little difference between the direct interpolation and the leveling approaches, when the data is misaligned. For both approaches, the absolute strain error is in excess of 2% near the holes, and approximately 22–24% of the specimen area has error above 4.2 times the strain resolution. Thus we see that while the leveling approach is able to

disentangle relevant strain errors due to model form error (e.g. incorrect boundary conditions) from false errors due to different filtering, it is not immune to false errors due to misalignment.

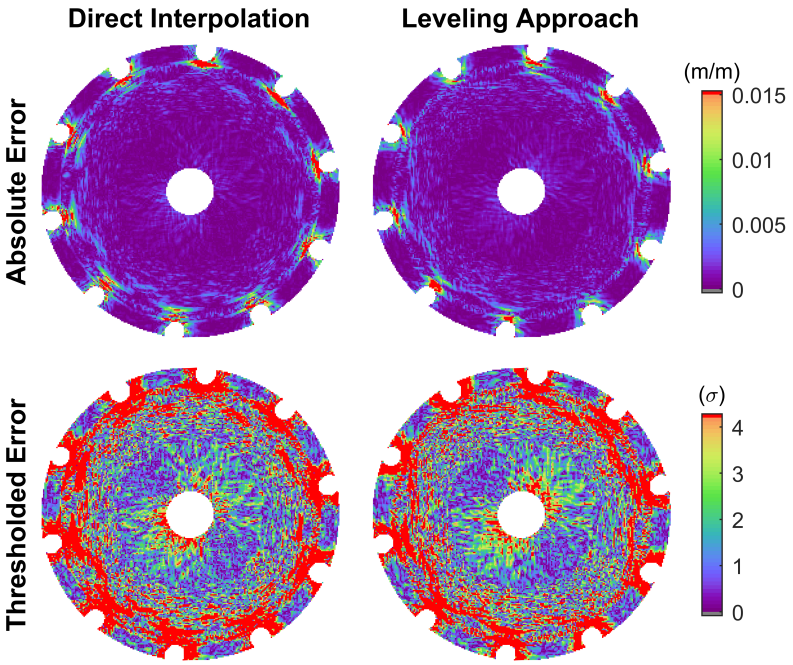

Figure 9: Strain error maps when the FEA data is misaligned with the "experimental" data. A VSG of 27 px was used for both the "experimental" and the leveled FE-DIC data.

Quantifying the magnitude of the strain errors caused by misalignment is difficult to do in a general way, but it is a combination of the spatial resolution of the DIC measurements and the spatial resolution of the strain features of interest. That is, misalignment has the largest effects in regions where there are sharp strain gradients in the specimen, such as near the holes in this example, while exact alignment is less critical if the strain gradients are small, such as in the interior of the specimen in this example. Knowing this, if evaluating sharp strain gradients were the main objective of a validation study, the experimental setup could be tuned to optimize the spatial resolution of the DIC measurements, by selecting a smaller field-of-view focused only on the region of the sample of high gradients. This magnification would reduce the strain gradient in terms of strain per pixel, making the validation studies less sensitive to misalignment errors of a few pixels magnitude. The increased magnification would also improve the spatial resolution of the DIC measurements, reducing the leveling effect of the DIC engine; a disadvantage, though, is the reduced field of view.

A second approach to improving alignment would be to first use DIC to measure the shape of the physical specimen. Then, one could create the FE geometry based on the DIC shape measurements. This process would inherently guarantee alignment between the FEA and the DIC data. Moreover, it would account for geometric imperfections in the as-built specimen, eliminating one possible source of model form error. However, disadvantages include the requirement to measure the entire specimen geometry (opposed to a select region-of-interest of the specimen), and the added complexity of the simulation workflow. In general, we believe that alignment between the FEA data and the experimental DIC data remains one of the key issues when generating full-field error maps for validation, and warrants further study to develop robust and precise methods of alignment.

6 Conclusions

This paper presents a thorough investigation of two different methods used to compute full-field error maps between experimental DIC data and FEA data, the so-called *direct interpolation approach* and the *DIC-*

leveling approach. While the two full-field validation approaches can be applied to any quantity-of-interest, we focused here on strain for demonstration purposes. With the *direct interpolation approach*, the strain is computed independently in either the FEA or the DIC software, on two independent grids or meshes. The data is then transferred from one mesh to the other using an interpolation scheme, and error maps are generated by subtracting the data on a point-by-point basis. While this method serves to place the two sets of data in the same coordinate system and on the same mesh, it fails to rectify several other important inconsistencies between the two sets of data, including different strain calculation algorithms, spatial resolutions and data filtering. To address these issues, we propose the *DIC-leveling approach*, in which the FEA data is processed through a DIC simulator, thereby leveling the FEA data to the DIC data in a regularization sense, and ensuring that both sets of data employ the same strain calculation algorithm and have the same spatial resolution and filtering.

To compare and contrast the two approaches systematically, an exemplar test case was chosen, of the cover plate of a pressure vessel. Bolt holes around the circumference of the cover plate and a connecter at the center induced stress concentrations, providing interesting features for the validation study. A reference FE analysis was created of the test specimen in Abaqus, and then a set of synthetically-deformed DIC images was generated using a stereo-DIC simulator in MatchID. We call the FEA-based synthetic image deformation process F-SID.

The images generated from F-SID served two purposes in this work. First, white Gaussian noise was added to the images to mimic image noise from an actual DIC measurement. These images were then treated as if they came from an actual experiment in the laboratory. Because these synthetic "experimental" images were derived from the reference FEA, though, they had no model form error. Second, the noise-free images were processed through a DIC engine to create DIC-leveled FEA data. This DIC-leveled FEA data was a convolution of the original FEA data and the filtering imposed by the DIC engine. In the end, three sets of full-field strain data were derived from the reference FEA: (1) Pure FEA strains, computed directly from the displacements exported from the FEA software; these strains were noise-free and had a virtual strain gauge (VSG) size of 3 pixels. (2) DIC-leveled FEA strains, computed from the noise-free F-SID images; these strains were also nearly noise free, but had a VSG size determined by the DIC processing parameters. (3) Synthetic "experimental" DIC strains, computed from the noisy F-SID images; these strains had noise typical of experiments, and also had a VSG size determined by the DIC processing parameters.

The two different full-field validation approaches were applied to compute full-field strain error maps, as the difference between the synthetic "experimental" DIC data and either the pure FEA data (for the direct interpolation approach) or the DIC-leveled FEA data (for the DIC-leveling approach). The error maps were created using three different virtual strain gauge sizes, to explore how the trade-off between strain resolution and spatial resolution affects the error maps and validation results. Given that the synthetic "experimental" data exactly encoded the original FEA data, the strain error should have been zero. However, with the direct interpolation approach, significant strain errors were computed, caused by neglecting the filtering effect of the DIC engine. That is, the "experimental" DIC strains had lower spatial resolution than the pure FEA strains, and thus the peak amplitudes of the strains near stress concentrations were underestimated, leading to an apparent disagreement with the FEA. In contrast, with the DIC-leveling approach, the exact same filtering was applied to both the synthetic "experimental" data as well as the DIC-leveled FEA data. In this case, no strain error was observed, as expected.

Next, we analyzed the effects of model form error, by specifically imposing a mismatch in boundary conditions between the FEA and the synthetic "experimental" data. This process mimicked the situation where one bolt was not fully torqued in the laboratory, but ideal boundary conditions (i.e. all bolts fully torqued) were applied to the FE model. When the direct interpolation approach was used, the effect of the loose bolt was completely obfuscated by the apparent errors introduced by neglecting the filtering effect of the DIC engine. There was no indication in the validation results that there was a mismatch in the boundary conditions between the "experimental" data and the FE model. In contrast, when the DIC-leveling approach was used, the strain error was concentrated near the loose bolt, with nearly zero error over the rest of the specimen. These results clearly and correctly elucidated a localized difference between the "experimental" and DIC-leveled FEA data, which is a key finding for a validation study.

Finally, we examined the effect of misalignment between the synthetic "experimental" data and the FEA data, by purposefully shifting the "experimental" data radially 4.2 px, or approximately 0.52 mm (less than 1% of the diameter of the pressure vessel cover), relative to the FEA data. Unfortunately, even such a small

misalignment had large effects on the strain error maps, particularly in regions where the strain gradients were high, i.e. near the bolt holes. Neither the direct interpolation nor the DIC-leveling approach was unable to disentangle relevant strain errors due to model from error from false errors due to misalignment. Thus, developing a robust and precise method to align experimental data to FEA data remains a significant challenge and warrants further study.

While these effects were demonstrated here with strain as the quantity-of-interest, similar considerations attend all DIC quantities-of-interest, such as displacement, velocity, acceleration, strain, strain-rate, etc. However, the magnitude of the leveling effect depends on the magnitude of the filtering the DIC engine imposes on each quantity-of-interest. Thus, for instance, one would expect a smaller difference between the direct interpolation approach and the DIC-leveling approach for displacements compared to strains, since the spatial resolution of displacements is typically smaller/better (on the order of the subset size) than the spatial resolution of strains (on the order of several subset sizes). That said, displacements are an integral quantity from the fundamental kinematic quantity-of-interest in the mechanics of deformable solids—strains. As such, displacements are poorly sensitive to local variations of deformation and are therefore typically not suitable to use for validation studies.

In summary, the results presented here highlight the fundamental importance of guaranteeing that the inconsistencies inherent between FEA and DIC data — namely strain calculation algorithm, spatial resolution, and data filtering — are rectified before full-field error maps are computed. If these issues are not addressed, apparent strain errors are computed, which may falsely lead an analyst to conclude that there is an error in the FEA, when in reality the apparent strain errors are caused only by neglecting to account for the filtering effect of the DIC engine. The leveling approach proposed here — in which the FEA data is processed through the same DIC engine as the experimental DIC data — addresses these issues by applying the same filtering to both sets of data, leading to accurate validation results.

Looking forward, while this paper focused on the effect of the DIC-leveling approach on validation studies, similar concepts could be applied to material model calibrations employing full-field experimental data. For instance, if finite-element model updating is used, where the cost function is built between the full-field DIC strains and the FEA strains, neglecting the filtering effect of the DIC engine could bias the calibration results. Additionally, the concept of the leveling approach developed here for DIC data could also analogously be applied to data generated from other types of full-field experimental techniques, such as the grid method. Leveling the FEA data to the experimental data in a regularization sense is critical for any application and any type of full-field data.

7 Acknowledgments

The authors gratefully acknowledge Dr. Phillip Reu at Sandia National Laboratories for insightful discussions. This work was supported in part by Sandia National Laboratories, a multimission laboratory managed and operated by National Technology and Engineering Solutions of Sandia, LLC, a wholly owned subsidiary of Honeywell International Inc., for the U.S. Department of Energy's National Nuclear Security Administration under contract DE-NA0003525. This paper describes objective technical results and analysis. Any subjective views or opinions that might be expressed in the paper do not necessarily represent the views of the U.S. Department of Energy or the United States Government.

References

[1] ASME. Guide for verification and validation in computational solid mechanics, 2016.

[2] E. Patterson, P. Brailly, and M. Taroni. High frequency quantitative photoelasticity applied to jet engine components. *Exp Mech*, 46:661–668, 2006.

[3] R.L. Burguete and E.A. Patterson. Comparison of numerical and experimental analyses for contact problems under normal and tangential loads. *P I Mech Eng G-J Aero*, 215(2):113–123, 2001.

[4] E.W. O'Brien. A better than average stress model — photoelastic analysis for airbus design. *P I Mech Eng G-J Aero*, 207(2):133–137, 1993.

[5] M.A. Sutton, J.J. Orteu, and H. Schreier. *Image Correlation for Shape, Motion and Deformation Measurements: Basic Concepts, Theory and Applications*. Springer US, 1 edition, 2009.

[6] M. Grédiac, F. Sur, and B. Blaysat. The grid method for in-plane displacement and strain measurement: A review and analysis. *Strain*, 52(3):205–243, 2016.

[7] C. Sebastian, E. Hack, and E. Patterson. An approach to the validation of computational solid mechanics models for strain analysis. *J Strain Anal Eng*, 48(1):36–47, 2012.

[8] W. Wang, J. E. Mottershead, C. M. Sebastian, and E. A. Patterson. Shape features and finite element model updating from full-field strain data. *Int J Solids Struct*, 48(11-12):1644–1657, 2011.

[9] W. Wang, J. E. Mottershead, and C. Mares. Mode-shape recognition and finite element model updating using the zernike moment descriptor. *Mech Syst Signal Pr*, 23(7):2088–2112, 2009.

[10] M. Salloum, K. L. Johnson, J. E. Bishop, J. M. Aytac, D. Dagel, and B. G. van Bloemen Waanders. Adaptive wavelet compression of large additive manufacturing experimental and simulation datasets. *Comp. Mech.*, 63(3):491–510, 2018.

[11] M. Salloum, E.M.C. Jones, D.M. Hensinger, and K. N. Karlson. Spatial error field reconstruction using Alpert multiwavelets. ASME V&V Symposium, Las Vegas, NV, May 2019.

[12] R. Balcaen, L. Wittevrongel, P. L. Reu, P. Lava, and D. Debruyne. Stereo-DIC calibration and speckle image generator based on FE formulations. *Exp Mech*, 57:703–718, 2017.

[13] MatchID. http://www.matchid.eu/ Accessed 22 May 2019.

[14] P. Lava, S. Cooreman, S. Coppieters, M. De Strycker, and D. Debruyne. Assessment of measuring errors in DIC using deformation fields generated by plastic FEA. *Opt Laser Eng*, 47:747–753, 2009.

[15] J.-E. Dufour, B. Beaubier, F. Hild, and S. Roux. CAD-based displacement measurements with stereo-DIC. *Exp Mech*, 55:1657–1668, 2015.

[16] L. Dubreuil, J.-E. Dufour, Y. Quinsat, and F. Hild. Mesh-based shape measurements with stereocorrelation. *Exp Mech*, 56:1231–1242, 2016.

[17] I. Konstantinou. *Development of a data-rich procedure to experimentally validation finite element simulation of engineering structures.* MSc thesis, 2013. University of Southampton, UK.

[18] M. Rossi, P. Lava, F. Pierron, D. Debruyne, and M. Sasso. Effect of DIC spatial resolution, noise, and interpolation error on identification results with the VFM. *Strain*, 51(3):206–222, 2015.

[19] M. Bornert, F. Brémand, P. Doumalin, J. C. Dupré, M. Fazzini, M. Grédiac, F. Hild, S. Mistou, J. Molimard, J. J. Orteu, L. Robert, Y. Surrel, P. Vacher, and B. Wattrisse. Assessment of digital image correlation measurement errors: Methodology and results. *Exp Mech*, 49(3):353–370, 2008.

[20] L. Wittevrongel, P. Lava, S. V. Lomov, and D. Debruyne. A self adaptive global digital image correlation algorithm. *Exp Mech*, 55(2):361–378, 2014.

[21] P. L. Reu, E. Toussaint, E.M.C. Jones, H.A. Bruck, M.A. Iadicola, R. Balcaen, D.Z. Turner, T. Siebert, P. Lava, and M. Simonsen. DIC challenge: Developing images and guidelines for evaluating accuracy and resolution of 2D analyses. *Exp Mech*, 58:1067–1099, 2018.

[22] P. Wang, F. Pierron, M. Rossi, P. Lava, and O.T. Thomsen. Optimised experimental characterisation of polymeric foam material using DIC and the virtual fields method. *Strain*, 52(1):59–79, 2016.

[23] E. M. C. Jones, K. N. Karlson, and P. L. Reu. Investigation of assumptions and approximations in the virtual fields method for a viscoplastic material model. *Strain*, 55(4), 2019.

[24] E.M.C. Jones, J.D. Carroll, K.N. Karlson, S.L.B. Kramer, R.B. Lehoucq, P.L. Reu, and D.Z. Turner. Parameter covariance and non-uniqueness in material model calibration using the virtual fields method. *Comp. Mater. Sci.*, 152:268–290, 2018.

[25] X. Gu and F. Pierron. Towards the design of a new standard for composite stiffness identification. *Compos Part A - Appl S*, 91:448–460, 2016.

[26] International Digital Image Correlation Society, E.M.C. Jones, and M.A. Iadicola. *A Good Practices Guide for Digital Image Correlation*. 1st edition, 2018. https://doi.org/10.32720/idics/gpg.ed1.

[27] P. Lava, F. Pierron, and P. L. Reu. DIC Course—Metrology Beyond Colors. Ghent, 2015.

[28] Bureau International des Poids et Mesures (BIPM). *JCGM 100:2008: Evaluation of measurement data — Guide to the expression of uncertainty in measurement*. 2008.

[29] P. L. Reu. A study of the influence of calibration uncertainty on the global uncertainty for digital image correlation using a Monte Carlo approach. *Exp Mech*, 53(9):1661–1680, 2013.